VŠB – Technická univerzita Ostrava

Elektronová struktura, fázová stabilita a optické vlastnosti cérem dopovaných fází TiO_2

Electronic structure, phase stability and optical properties of Ce-doped TiO_2 phases

2015

Author: Lukáš Sojka

Supervisor: Ing. Dominik Legut, Ph.D.

VŠB - Technical University of Ostrava
University Study Programmes
CNT - Nanotechnology Centre

Bachelor Thesis Assignment

Student: **Lukáš Sojka**

Study Programme: B3942 Nanotechnology

Study Branch: 3942R001 Nanotechnology

Title: Elektronová struktura, fázová stabilita a optické vlastnosti cérem dopovaných fází TiO_2
Electronic structure, phase stability and optical properties of Ce-doped TiO_2 phases

Description:

In last two decades an enormous scientific interest has been devoted to the investigation of the photoactivity of titania crystalline polymorphs such as anatase, brookite and rutile and their mixtures under UV light. From the recent experimental works supported by theoretical calculations two of the routes enhance visible-light photoactivity [2]. At first by a production of large oxygen deficient TiO_2 phases. However, oxygen vacancies have short lifetime, i.e. they are not thermodynamically stable. At second, by doping of the lathanides [3], such as cerium [4]. The Ce has competing itinerant vs. localized behavior of electrons in d- and especially f-shell and hence variable valence states (Ce^{3+}/Ce^{4+}). In this theme the role of the Ce in bulk TiO_2 phases by means of the electronic-structure related properties is determined by first-principles calculations. Primarily, the phase stability, the optical properties and the influence of the various Ce valence states on energetics, band gaps, etc. will be investigated.

References:

1. FUJISHIMA, A., X. ZHANG, D. A. TRYK. Surf. Sci. Rep., 2008, Vol. 63, pp. 515-582.
2. JUSTICIA, I., P. ORDEJON, G. CANTO, J. L. MOZOS, A. FIGUERAS. Advanced Materials, 2002, 14, 1399.
3. BINGHAM, S., W.A. DAOUD. J. Mater. Chem., 2011, 21, 2041.
4. ŠTENGL, V., S. BAKARDJIEVA, N. MURAFA. Mater. Chem. Phys., 2009, Vol. 114, pp. 217-226.

Extent and terms of a thesis are specified in directions for its elaboration that are opened to the public on the web sites of the Nanotechnology Centre.

Supervisor: **Ing. Dominik Legut, Ph.D.**

Date of issue: 20.10.2014

Date of submission: 15.05.2015

prof. Ing. Jaromír Pištora, CSc.
Head of Department

VYSOKÁ ŠKOLA BÁŇSKÁ - TECHNICKÁ UNIVERZITA OSTRAVA UNIVERZITNÍ STUDIJNÍ PROGRAMY

prof. Ing. Petr Noskievič, CSc.
Vice-rector for Study Affairs

Prohlášení

- Byl jsem seznámen s tím, že na moji bakalářskou práci se plně vztahuje zákon č.121/2000 Sb. – autorský zákon, zejména § 35 – využití díla v rámci občanských a náboženských obřadů, v rámci školních představení a využití díla školního a § 60 – školní dílo.

- Beru na vědomí, že Vysoká škola báňská – Technická univerzita Ostrava (dále jen VŠB-TUO) má právo nevýdělečně, ke své vlastní potřebě, bakalářskou práci užít (§ 35 odst. 3)

- Souhlasím s tím, že jeden výtisk bakalářské práce bude uložen v Ústřední knihovně VŠB-TUO k prezenčnímu nahlédnutí a jeden výtisk bude uložen u vedoucího bakalářské práce. Souhlasím s tím, že údaje o bakalářské práci obsažené v Záznamu o závěrečné práci, budou zveřejněny v informačním systému VŠB-TUO.

- Místopřísežně prohlašuji, že celou bakalářskou práci, včetně příloh, jsem vypracoval samostatně a uvedl jsem všechny použité podklady a literaturu.

V Ostravě dne 15.5.2015

_____

Declaration

- I hereby declare that I elaborated this bachelor thesis by myself. All the literary sources and publications used in this work have been cited.

Ostrava, May 15, 2015

_____

Abstrakt

Tato bakalářská práce je zaměřena na teoretické *ab-initio* výpočty fází oxidu titaničitého dopovaného cerem. V této práci jsou studovány anatas a brookite, což jsou tetragonální, respektive ortogonální polymorfy TiO_2. Po optimalizaci parametrů výpočtů, byly vypočteny vlastnosti základního stavu TiO_2 fází. Dále byly studovány komplexní sloučeniny titanu a ceru s důrazem na fázovou stabilitu těchto sloučenin. Byla vypočtena elektronová struktura a optické vlastnosti s ohledem na předpokládanou fotokatalytickou aktivitu. Veškerá vypočtená data byla získána pomocí balíku Vienna *Ab-initio* Simulation Package (VASP).

Abstract

This bachelor thesis is focused on theoretical *ab-initio* calculations of cerium doped titanium dioxide phases. The ones studied in this work are anatase and brookite, tetragonal and orthogonal polymorphs, respectively. After the optimization of computational paremetres, the ground-state properties were determined. Other complex compounds regarding titanium and cerium were also studied with emphasis on phase stability of those compounds. The electronic structure and optical properties were calculated as well, to address the possibility of photocatalytic activity. All the data gathered were obtained using Vienna *Ab-initio* Simulation Package (VASP).

Contents

1. Introduction

Titanium dioxide has three most commonly occurring crystallographic modifications in nature. Those three are anatase, brookite and rutile. [1] There are also some other possible phases under more drastic conditions, such as high pressure and temperature. [2] Titanium dioxide is known to have multiple useful properties and therefore has been studied intensively in the last decades. [3,4] The most important property is catalysis and photocatalysis in particular. [5]

There are various approaches how to improve its photoactivity and broaden its range from UV also to visible-light spectra. [6] One of them is to synthesize titanium dioxide with large oxygen deficiency, which is however short-living. Another possibility is doping with lanthanides such as cerium. [7] Cerium has several specific advantages, mainly multi-electrons energy levels consisting of *d* and *f* orbitals and also variable valence-states associated with Ce^{3+}/Ce^{4+} redox processes. [8]

The aim of this work is to determine the electronic structure, i.e. ground-state of cerium-doped titania, also phase stability from calculations of enthalpy of formation and finally some basic optical properties to address the possibility of photocatalytic activity.

In Section 2 we present the methodology used in this work, our results are gathered in Section 3 and in Section 4 is the summary of this work.

2. Methodology

2.1. Quantum Theory of Solids

2.1.1 The Many-Body Equation

All the data gathered in this work were calculated using *ab-initio* approach. It means that we start from the quantum mechanical description of the matter. The state and all other observable properties of the matter are determined completely by **Schrödinger equation**. Its exact formulation is also known as the many-body equation: [9]

$$\mathcal{H}\Psi(\{r_i\},\{R_\alpha\},t) = i\hbar\frac{\partial\Psi}{\partial t} \qquad 2.1$$

where $\boldsymbol{\mathcal{H}}$ is the exact many-body Hamiltonian and the wavefunction Ψ is a function of all electronic and nuclear coordinates denoted by r_i and R_α respectively. As there are of the order 10^{25} of electrons and 10^{24} of nuclei mutually interacting with each other, none of them moving at a velocity anywhere close to the speed of light, we can approximate the Hamiltonian to be the sum of nonrelativistic kinetic energies and Coulomb interactions of the electrons and ion cores: [9]

$$\mathcal{H} = \sum_i \frac{{p_i}^2}{2m} + \sum_\alpha \frac{{p_\alpha}^2}{2M_\alpha} + \frac{1}{2}\sum_{i,j}\frac{e^2}{|r_i - r_j|} + \frac{1}{2}\sum_{\alpha,\beta}\frac{Z_\alpha Z_\beta e^2}{|R_\alpha - R_\beta|} - \sum_{i,\alpha}\frac{Z_\alpha e^2}{|r_i - R_\alpha|} \qquad 2.2$$

where p_i and P_α are the momenta of the electrons and ion cores, respectively, m is the mass of electron, M_α is the mass of the ion core at position R_α and Z_α is the respective charge. Indices i and j sum the electrons, while α and β sum the ion core. The left side of the equation represents, respectively, the kinetic energies of electrons and ion cores, the repulsive Coulomb potential between the electrons and similarly for ion cores and finally the attractive Coulomb potential energy between electrons and ion cores. [9]

With an equation given as it is, we already face the problem of separating the electrons in each atom into valence ones, which have the explicit coordinates r_i in the formula above, and core ones, which are a part of the ion core and stick together with the nucleus all the time. [9]

2.1.2 Adiabatic Approximation

Based on perturbation theory and separation of variables, it solves Schrödinger equations for electronic and nuclear coordinates separately. The electron coordinates only equation is as follows: [9]

$$\left\{\sum_i \frac{{p_i}^2}{2m} + \frac{1}{2}\sum_{i,j}\frac{e^2}{|r_i - r_j|} - \sum_{i,\alpha}\frac{Z_\alpha e^2}{|r_i - R_\alpha|}\right\}\varphi_n = E_n\varphi_n, \qquad 2.3$$

while the nuclear coordinates only equation is:

$$\left\{\sum_\alpha \frac{{p_\alpha}^2}{2M_\alpha} + \frac{1}{2}\sum_{\alpha,\beta}\frac{Z_\alpha Z_\beta e^2}{|R_\alpha - R_\beta|} + E_n(\{R_\alpha\})\right\}\Psi_n = E_{n,\lambda}\Psi_{n,\lambda}, \qquad 2.4$$

where $\varphi_n = (\{r_i\};\{R_\alpha\})$ and $\Psi_{n,\lambda} = (\{R_\alpha\})$ are eigenfunctions and $E_n(\{R_\alpha\})$, $E_{n,\lambda}(\{R_\alpha\})$ are their respective eigenvalues. Their solutions are orthonormal and thus form the adiabatic basis. The adiabatic approximation, also called **Born-Oppenheimer approximation**, assumes that the ion cores continuously deform the electronic wavefunctions and the electrons only provide a potential energy for the ion-core motion. [10]

2.1.3 The Ion-Core Schrödinger Equation

Assuming that the electronic problem in equations above can be solved for any arrangement of electrons, we can rewrite it into the following form: [9]

$$\left[\sum_\alpha \frac{{p_\alpha}^2}{2M_\alpha} + V_n(\{R_\alpha\})\right]\Psi_{n,\lambda} = E_{n,\lambda}\Psi_{n,\lambda} \qquad 2.5$$

where the total potential of the cores is given by the summation of their mutual Coulomb repulsion and the potential due to the electronic motion: [9]

$$V_n(\{R_\alpha\}) = \frac{1}{2}\sum_{\alpha,\beta}\frac{Z_\alpha Z_\beta e^2}{|R_\alpha - R_\beta|} + E_n(\{R_\alpha\}). \qquad 2.6$$

2.1.4 The Structure of Solids

Considering the state belonging to n=0 (the ground state of each electron), the solution of equation (2.5) yields eigenvalues of $E_{0,\lambda}$. The ground-state energy is then $E_{0,0}$ belonging to eigenfunction $\Psi_{0,0}$. Assuming that Born-Oppenheimer approximation is valid, the function V_0 must have absolute minima in each coordinate R_α. Thus there is an equilibrium configuration for the ion-cores, which we call the structure of the solid. There are also other local minima for most materials, allowing them to appear in various allotropic modifications. [9,11]

Most of the solids have the equilibrium configuration possessing long-range periodicity and we call them crystals. Those are described by their lattice (periodic array of positions) and a basis (set of atoms associated with each lattice point). Note that some materials have their ground state in the amorphous or quasicrystalline form. [9,11]

2.2. Density Functional Theory

There are two main paths, which both emerged from quantum mechanics, to determine the electronic structure of materials. One of them is Hartree and Hartree-Fock approximation, more popular amongst the quantum chemists and the Density Functional Theory, widely used in computing the properties of solids. First of all, let's start with the Hartree approximation. [9]

2.2.1 The Hartree Approximation

This approximation is based on solving the Schrödinger equation using variational principle. We assume that the wavefunction φ of the whole system can be obtained from the combination of wavefunctions Φ, each representing one of the *n* particles. [9]

$$\varphi(\{r_i\}) = \Phi_1(r_1)\Phi_2(r_2) \dots \Phi_n(r_n) \qquad 2.7$$

The next step is minimizing the energy of the Hamiltonian with respect to variations in Φ_i. We get an effective Schrödinger equation for each of the Φ_i: [9]

$$\left[-\frac{\hbar^2}{2m}{\nabla_i}^2 + e^2\sum_{j\neq i}\int\frac{\left|\Phi_j(r)\right|^2}{|r_i - r|}dr - e^2\sum_{\alpha}\frac{Z_\alpha}{|r_i - R_\alpha|}\right]\Phi_i(r_i) = \varepsilon\Phi_i(r_i) \qquad 2.8$$

where the integration in the Coulomb term is there to include the spin inner product. The first term from the left is the kinetic energy, the next one stands for Coulomb potential generated by all other electrons and the third one is for the attractive Coulomb potential generated by the ion cores. The major drawback of this approximation is that it does not take the antisymmetric statistics of the electrons into account. Moreover it drastically underestimates the cohesion. [9]

2.2.2 The Hartree-Fock Approximation

Taking the assumptions made in the Hartree approximation and adding antisymmetry into the wavefunction makes together the Hartree-Fock approximation. If we interchange the particles, the *n*-electron wavefunction is then antisymmetric, which comes out of the Slater determinant: [9]

$$\varphi(\{r_i\}) = \frac{1}{\sqrt{n!}}\begin{vmatrix}\Phi_1(r_1) & \Phi_1(r_2) & \cdots & \Phi_1(r_n)\\ \Phi_2(r_1) & \Phi_2(r_2) & \cdots & \vdots\\ \vdots & \vdots & \ddots & \vdots\\ \Phi_n(r_1) & \cdots & \cdots & \Phi_n(r_n)\end{vmatrix} \qquad 2.9$$

A modified Hamiltonian acquired through minimization looks like this:

$$\left[-\frac{\hbar^2}{2m}{\nabla_i}^2 + e^2\sum_{j}\int\frac{\left|\Phi_j(r_j)\right|^2}{|r_i - r_i|}dr_j - e^2\sum_{\alpha}\frac{Z_\alpha}{|r_i - R_\alpha|}\right]\Phi_i(r_i) - e^2\sum_{j}\int\frac{{\Phi_j}^*(r)\Phi_j(r_i)\Phi_i(r)}{|r_i - r_j|}dr_j = \varepsilon\Phi_i(r_i) \qquad 2.10$$

where the first three terms are the same as in the Hartree approximation and the integration is understood in the same way. The fourth term is called the **exchange term** and is the product of the antisymmetrized wavefunction. The difference between exact energy of the system and the energy calculated by the Hartree-Fock approximation defines the **correlation energy**. [9]

2.2.3 Basic Density Functional Theory

Kohn, Sham and Hohenberg [12,13] proposed a theorem stating that the total energy E of the system is determined only by the electron density ρ of its ground state:

$$E = E[\rho(r)] \tag{2.11}$$

and that the ground state energy minimizes this functional as follows:

$$\left.\frac{\partial E[\rho]}{\partial \rho}\right|_{\rho 0} = 0 \tag{2.12}$$

where ρ_0 is the exact electron density of the many-body ground state.

This causes a tremendous simplification of the problem, since it reduces the number of degrees of freedom from original $3N$, where $N \sim 10^{24}$, to only 3 degrees of freedom in three-dimensional space. All the thermodynamical properties of the electron gas are then described by its density. We have to remember that the electron density is also determined by the positions of the ion-cores:

$$E = E[\rho(r; \{R_\alpha\})] \tag{2.13}$$

where R_α stands for the degrees of freedom. [9]

The Kohn-Sham-Hohenberg theorem is applied to solve the electronic Schrödinger equation in a way that each electron is viewed as it is moving in an effective field with effective potential V_{eff} of the other electrons and ion-cores. This implies that the potential is given self-consistently, since the wavefunction for each electron is a part of the effective potential of all other electrons. The Schrödinger equation determining the effective electrons' wavefunctions in the general form: [9]

$$\left[-\frac{\hbar^2}{2m}\nabla^2 + V_{eff}\right]\Psi_i(r) = \varepsilon_i \Psi_i(r) \tag{2.14}$$

where the Ψ_i produce the exact charge density:

$$\rho(r) = \sum_i n_i |\Psi_i(r)|^2 \tag{2.15}$$

with the occupation number of the i-th state. The total energy is expressed as follows:

$$E = T + e^2 \int \frac{\rho(r)\rho(r')}{|r - r'|} dr dr' - e^2 \sum_{\alpha} \int \frac{Z_\alpha \rho(r)}{|R_\alpha - r|} dr + E_{xc}(\rho) \qquad 2.16$$

The second and third terms on the right-hand side of the equation are the Coulomb repulsion between electrons and Coulomb attraction between electrons and ion-cores, respectively. The last term is the exchange-correlation energy, which is the reduction of the total energy due to the reduced repulsion between electrons with parallel and anti-parallel spins. The term T stands for the sum of kinetic energies of the effective electrons (whose density is the same as with the real electrons, but represent independent electrons in effective field): [9]

$$T = -\frac{\hbar^2}{2m} \sum_i n_i \int \Psi_i^*(r)\, \nabla^2 \Psi_i(r) dr. \qquad 2.17$$

2.2.4 Kohn-Sham Equations

Having the expression (2.16), we shall now proceed with getting more practical use of the density functional theory. Furthermore, substituting (2.16) and (2.15) into (2.12) and interpreting it with respect to ρ as a variation of each Ψ_i gives us the following form of (2.14):

$$\left[-\frac{\hbar^2}{2m} \nabla^2 + V_{eff} \right] \Psi_i(r) = \varepsilon_i \Psi_i(r) \qquad 2.18$$

where the effective potential is given by: [9]

$$V_{eff} = V_C(r) + V_{xc}[\rho(r)] \qquad 2.19$$

which is the sum of Coulomb and exchange-correlation potentials. We call these the **Kohn-Sham** equations. The ground-state density, given by solution of these equations, forms the orthonormal basis: [9]

$$\int \Psi_i^*(r) \Psi_j(r) dr = \delta_{i,j} \qquad 2.20$$

The Lagrange multipliers, which appear as the eigenvalues of the Ψ_i, assure this condition.

The equation (2.16) yields the following Coulomb potential: [9]

$$V_C(r) = -e^2 \int \frac{\rho(r')}{|r - r'|} dr + e^2 \int \frac{Z_\alpha}{|R_\alpha - r|} \qquad 2.21$$

The exchange-correlation potential V_{xc} is in relation with the exchange-correlation energy by:

$$V_{xc} = \frac{\partial E_{xc}}{\partial \rho} \qquad 2.22$$

2.2.5 The Local Density Approximation

This approximation is obtained by the assumption that E_{xc} is depending only on the local value of ρ: [9]

$$E_{xc}{}^{LDA} = \int \rho(r)\varepsilon_{xc}(r)\, dr \qquad 2.23$$

The two basic assumptions are that the exchange-correlation effects are dominated by the density in immediate vicinity of point r and that these effects do not vary strongly with position. The LDA is accurate for many metallic materials, but stops being accurate in systems with strong electron density variations, such as systems involving f-electrons. The ε_{xc} has been studied using a few different approaches in a system of interacting electrons on a background of homogenous positive charge. This was called the **homogenous electron gas** and the ε_{xc} has been determined for a range of densities. [9]

2.2.6 Generalized Gradient Approximation

This is an improvement of the Local Density Approximation, since it takes the dependence of the exchange-correlation energy on the gradient of the density into account: [9]

$$E_{xc}{}^{GGA} = \int f[\rho(r), \nabla\rho]\, dr \qquad 2.24$$

and thus it is being called "non-local" sometimes. This method was successful in description of spin-polarized ground state of bcc Fe. [9,14]

2.2.7 Augmented Plane Wave Method

This method (APW) was introduced by Slater in 1937. [15] The idea behind this method is the partitioning of the space around atoms into continuous spheres and interstitial region. The Schrödinger equation is re-written into spherical polar coordinates and the radial and angular

variables are separated. The eigenfunctions are a product of the radial function $R_{nl}(r)$, which must be solved numerically and the spherical harmonics $Y_{lm}(\theta, \Phi)$: [9]

$$\Psi(r) = R_{nl}(r)Y_{lm}(\theta, \Phi) \qquad 2.25$$

The solutions in the interstitial region, after replacing the potential by a constant, are plane waves:

$$\Psi(r) = e^{ik \cdot r} \qquad 2.26$$

This defines a basis, which allows us to represent any potential as a superposition of those plane waves. [9]

2.2.8 The Pseudopotential Method

The basic presumption of this method is that the core electrons are not important for most of the important physical properties. Those electrons could be then put together with the nucleus to create pseudopotential in such a way, that the outer electrons do not differ from the electrons in the all-electron calculation. The pseudowavefunctions are much smoother in comparison with the real ones, because they have finite pseudopotential near the nucleus, which is in contrast with real wavefunctions. The pseudopotential method is particularly successful in description of electronic structure of semiconductors and also much less computationally demanding. [16]

2.3. Vienna *Ab-initio* Simulation Package

This is usually abbreviated as VASP. It is a complex package, which allows its users to perform various tasks concerning *ab-initio* quantum-mechanical molecular dynamics. In order to facilitate such tasks, it uses either projector-augmented wave method and corresponding plane wave basis set, or pseudopotentials (usually GGA or LDA). Its performance is optimized using many sophisticated features in the computing algorithm, ensuring fast convergence of the iteration cycles. [17]

To run calculations in VASP, one has to enter only five input files: POSCAR describing the structure of selected material including atomic positions and size of unit cell, POTCAR

which contains pseudopotential data, KPOINTS determining the sampling of the Brillouin zone, INCAR file, where the parametres of the calculation are written under corresponding "flags" and finally a script, which starts the calculation, usually by sending it into the queueing system. [17]

2.4. Modeled Quantities

There are many quantities that can be modelled with the help of first-principles calculations. For our purposes only a few of them are needed.

2.4.1 Bulk Modulus

Bulk modulus of the given material represents its resistance to uniform compression:

$$B = -V\frac{\partial p}{\partial V} = V\frac{\partial^2 E_{tot}}{\partial V^2} \qquad 2.27$$

where V is the volume, p is pressure and E_{tot} is total energy E-E_{min}. In order to obtain this quantity, one has to compose an energy-volume curve from static calculations. The unit is Pascal. [18]

2.4.2 Enthalpy of Formation

The enthalpy of formation (ΔH_f^0 at 0K) is defined as the total energy difference between the compound and the constituent elements. [18] We often drop the upper index 0, because our calculations are always at 0K. For brookite, the following formula was used:

$$H_f = E_{tot}(brookite - nCe) - nE_{tot}(fcc\ Ce) - mE_{tot}(hcp\ Ti) - kE_{tot}(O_2) \qquad 2.28$$

where E_{tot} is the total energy of the supercell of doped phase or the total energy of the respective phase. The n,m,k are the number of constituents, atomic species, respectively. Similar formula was used for Ce doped anatase phase.

2.4.3 Optical Properties

The optical properties in anisotropic materials are given by the complex refractive index or the permittivity/conductivity tensor. Thus the permittivity tensor ε is divided into ε_1 and ε_2 for real and imaginary part, respectively. The relation between those components is called the Kramers-Krönig relations.

Kramers-Krönig Relations

$$\varepsilon_1(\omega) = \varepsilon_0 + \frac{2}{\pi}\mathcal{P}\int_0^\infty \frac{\omega'\varepsilon_2(\omega')d\omega'}{\omega'^2 - \omega^2} \qquad 2.29$$

$$\varepsilon_2(\omega) = -\frac{2}{\pi}\mathcal{P}\int_0^\infty \frac{\varepsilon_1(\omega')d\omega'}{\omega'^2 - \omega^2} \qquad 2.30$$

where ω is angular frequency and Ƥ is Cauchy principal value. [19]

Reflectivity and energy-loss function

The frequency-dependent complex permittivity tensor is obtained from our *ab-initio* calculations. Having this, one can obtain the following expressions of reflectivity *R(ω)* and energy-loss function *L(ω)*: [20]

$$R(\omega) = \frac{\sqrt{\varepsilon(\omega) - 1}}{\sqrt{\varepsilon(\omega) + 1}} \qquad 2.31$$

$$L(\omega) = -Im\left|\frac{1}{\varepsilon(\omega)}\right| = \frac{\varepsilon_2(\omega)}{{\varepsilon_1}^2(\omega) + {\varepsilon_2}^2(\omega)} \qquad 2.32$$

3. Results

3.1. Computational Details

For our first-principles calculations, we adopted the VASP package [17], a plane-wave pseudopotential DFT code, within the single-electron framework. Projector-augmented-wave pseudopotentials (PAWs) were used for O, Ce, and Ti atoms with the valence configurations of $2s^2 2p^4$, $6s^2 5d^1 4f^1 4d^{10}$ and $3p^6 4s^2 3d^2$, respectively. General gradient corrected exchange-correlation functionals parametrized by Perdew‐Burke‐Ernzerhof (PBE) [14] and the plane-wave cut-off of 600 eV were used.

Calculations for anatase were carried within 3x3x1 supercells containing 108 atoms, see Fig. 2. Each supercell was sampled with the k-point mesh of 4x4x4 generated according to the scheme proposed by Monkhorst and Pack [21], whereas calculations for brookite were carried within 1x2x2 supercell (Fig. 3) containing 96 atoms in total. The k-points mesh of 2x2x2 for brookite was generated according to the same scheme. The convergence criteria for the total energies and forces in each supercell were set to 10^{-4} eV and 10^{-3} eV/Å, respectively.

3.2. Constituents

The ground-state structures of individual elements were determined. We had to optimize the parameters of our calculations, such as the energy cutoff and the number of *k*-points, to get the same structures as those reported by experimental works. It is important to identify the ground-state of cerium, since it occurs in many possible allotropic modifications.

3.2.1 Cerium

Cerium possesses various structures under pressure and temperature. It was reported to appear in body centered cubic (bcc), face centered cubic (fcc) and also unusual double hexagonal close packed (dhcp) structures. [22] We computed bcc, fcc and dhcp in both Ce^{3+} and Ce^{4+} valence states and the results are shown in Figure1:

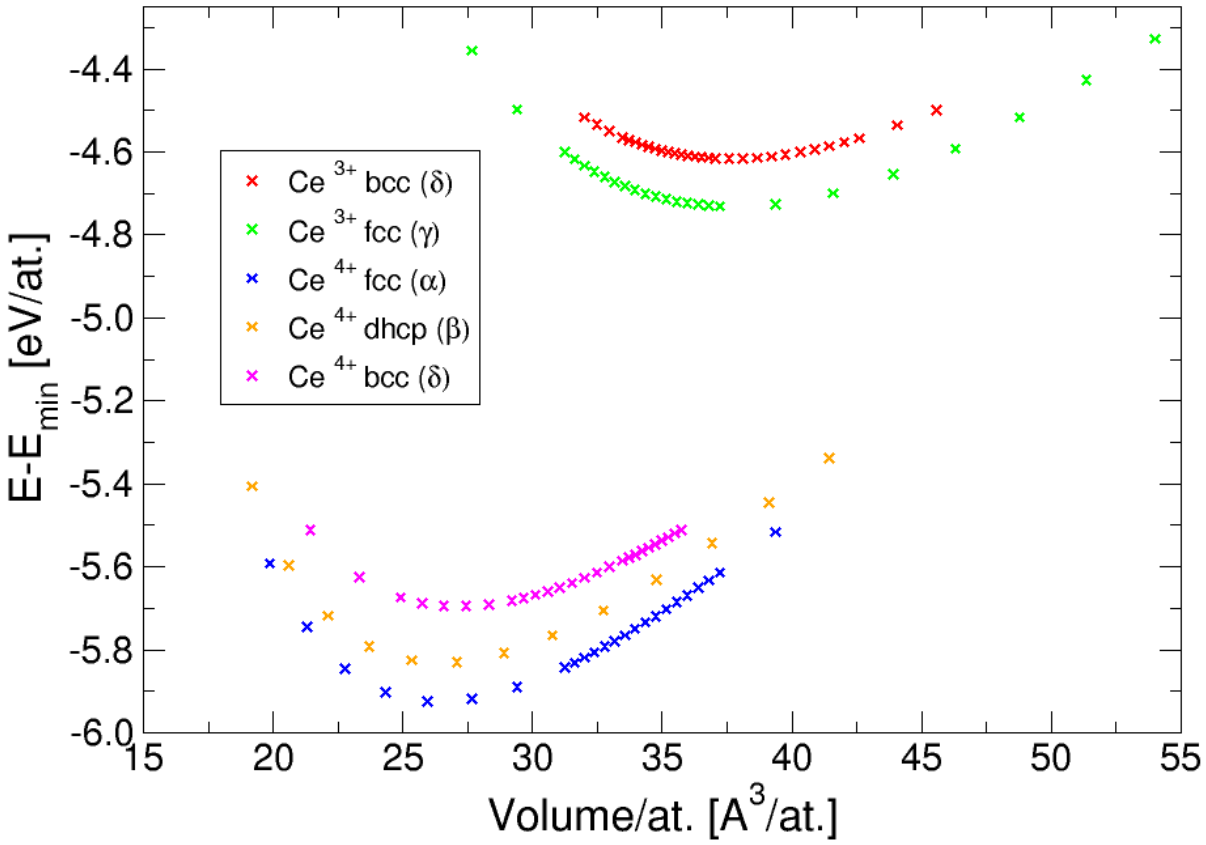

Figure 1: Energy-volume curves of selected Ce phases.

As we can see here, Ce^{4+} is always energetically preferred over Ce^{3+}, while the fcc structure is the most stable phase. It is a known fact, that Ce^{3+} and Ce^{4+} co-exist next to each other and create a redox potential. [8]

Our results lead to lattice constants $a(Ce^{3+})$=5.324Å and $a(Ce^{4+})$=4.729Å. It is in good agreement with experimental results - $a(Ce^{3+})$=5.161Å and $a(Ce^{4+})$=4.850Å respectively. [22]

3.2.2 Titanium

Determining the ground state of titanium was a simpler task, because of its hcp (hexagonal close packed) structure. The lattice constant a from our calculations is a=2.85Å and c/a=1.61. This is in good agreement with the experiment a=2.91Å and c/a=1.58. [23]

3.2.3 Oxygen

In contrast to previous two elements, oxygen is not a solid bulk material, for whom is VASP best suited. Luckily, one can solve this problem even for a molecule of two atoms, despite the increase in computational effort by requiring lots of planewaves in an empty box. In order to do so, one has to place the molecule into a box big enough, that there is effectively no interaction between molecules in neighbouring cells. In our calculation, we used cell approximately 10Å across all dicections. The computed equilibrium distance – a=1.22Å – between oxygen atoms in the dimer is in very good agreement with the experimental value – a=1.21Å. [23]

	Present work		Experiment	
	a [Å]	c/a	a [Å]	c/a
Ti (hcp)	2.85	1.61	2.91	1.58
O_2	1.22	-	1.21	-
Ce^{3+} (fcc)	5.32	-	5.16	-
Ce^{4+} (fcc)	4.73	-	4.85	-

Table 1: Summary of lattice parametres of constituents. [22, 23]

3.3. Titanium Dioxide

Let us remind that titanium dioxide has three most common polymorphs in nature: anatase, brookite and rutile. [1] In this work we are going to focus only on anatase and brookite. Anatase is a tetragonal form of TiO_2 with 12 atoms in the unit cell, while brookite is its orthogonal variant with 24 atoms in the conventional unit cell. At first we modeled those phases in pristine form, so that we can compare its properties with those phases doped with cerium and to track possible trends in changes of these properties.

Brookite	Present work	Experiment
a [Å]	9.253	9.191
b [Å]	5.497	5.439
c [Å]	5.174	5.144
Ti (8c)	(0.375, 0.129, 0.093)	(0.362, 0.130, 0.103)
O_1 (8c)	(0.197, 0.010, 0.351)	(0.183, 0.009, 0.348)
O_2 (8c)	(0.049, 0.230, 0.108)	(0.040, 0.226, 0.120)
H_f [eV/at.]	-3.435	
Anatase	Present work	Experiment
a,b [Å]	3.801	3.812
c [Å]	9.707	9.634
Ti (4b)	(0, 0.25, 0.375)	(0, 0.25, 0.375)
O (8e)	(0, 0.25, 0.169)	(0, 0.25, 0.167)
H_f [eV/at.]	-3.449	

Table 2: Comparison of lattice parametres and atomic positions with experimental data. [24,25] Calculated enthalpy of formation is also determined.

The calculated and experimentally determined lattice constants, Wyckoff positions and enthalpy of formation are summarized in Table 2. For both brookite and anatase phases, lattice constants are in very good agreement with experiment.

3.3.1 Effect of Concentration of Doped Cerium

With pristine dioxide successfully modeled, the next step was to start doping it with cerium. We extended our unit cells into bigger supercells, which allowed us to reach concentrations as low as approximately 1% at. That means we formed a 1x3x3 supercell of anatase with 108 atoms and 2x2x1 supercell of brookite with 96 atoms in it.

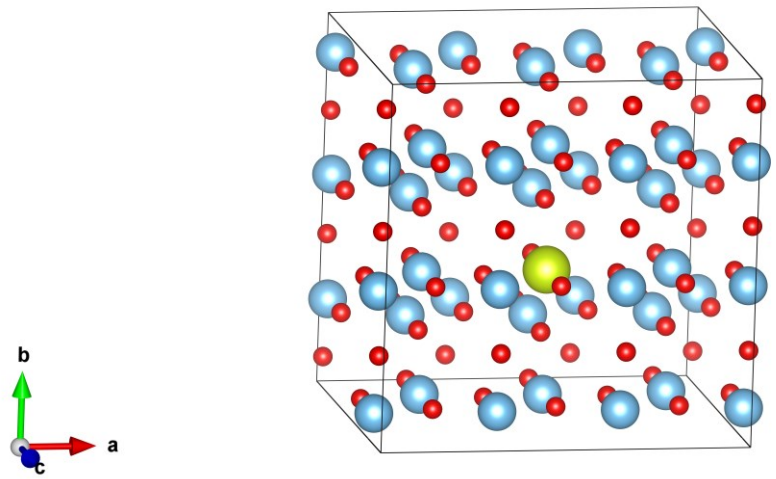

Figure 2: Supercell of 3x3x1 of anatase structure with 1 Ce atom. Blue atoms represent titanium, red ones oxygen and finally the green one is the cerium atom.

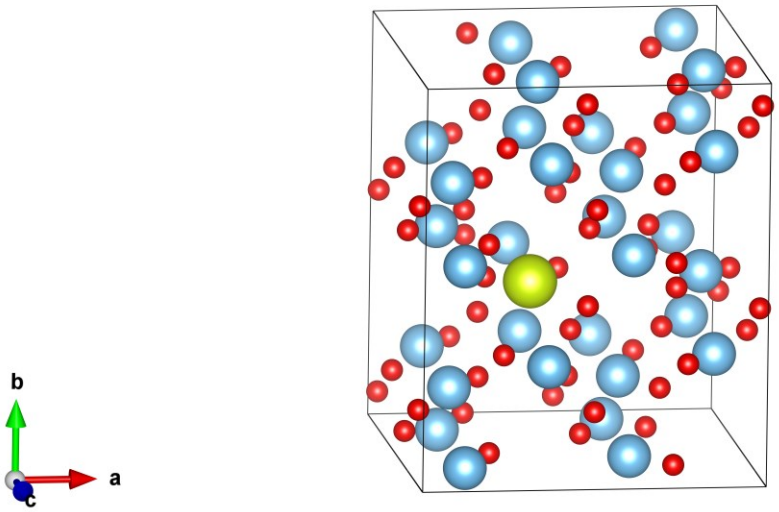

Figure 3: Supercell of 1x2x2 of brookite structure with 1 Ce atom. The colors are similar to Figure 2.

The doping with cerium was performed only by substituting the titanium atoms. The change in lattice parametres on the concentration of doped cerium atoms is shown in Table 3:

Ce concentration (at.%)	a [Å]	b [Å]	c [Å]
Brookite			
0.00	9.253	5.497	5.174
1.04	9.312	5.531	5.203
6.25	9.639	5.638	5.295
Anatase			
0.00	3.801	3.801	9.707
0.93	3.813	3.813	9.776
4.63	3.877	3.857	10.099

Table 3: Lattice parametres of anatase and brookite for selected concentrations of Ce.

The cell is expanding in all three directions as the concentration raises. That is probably because of more electrons in Ce in comparison with Ti, causing bigger atomic radius. The data utilized in Table 3 are from our calculations with doping of Ce with valence 4+. Cerium with valence 3+ would show even bigger increase in volume, because one additional electron in valence leads to the higher radius, as could be seen from the larger lattice constant of pure fcc structure of cerium 3+ as well.

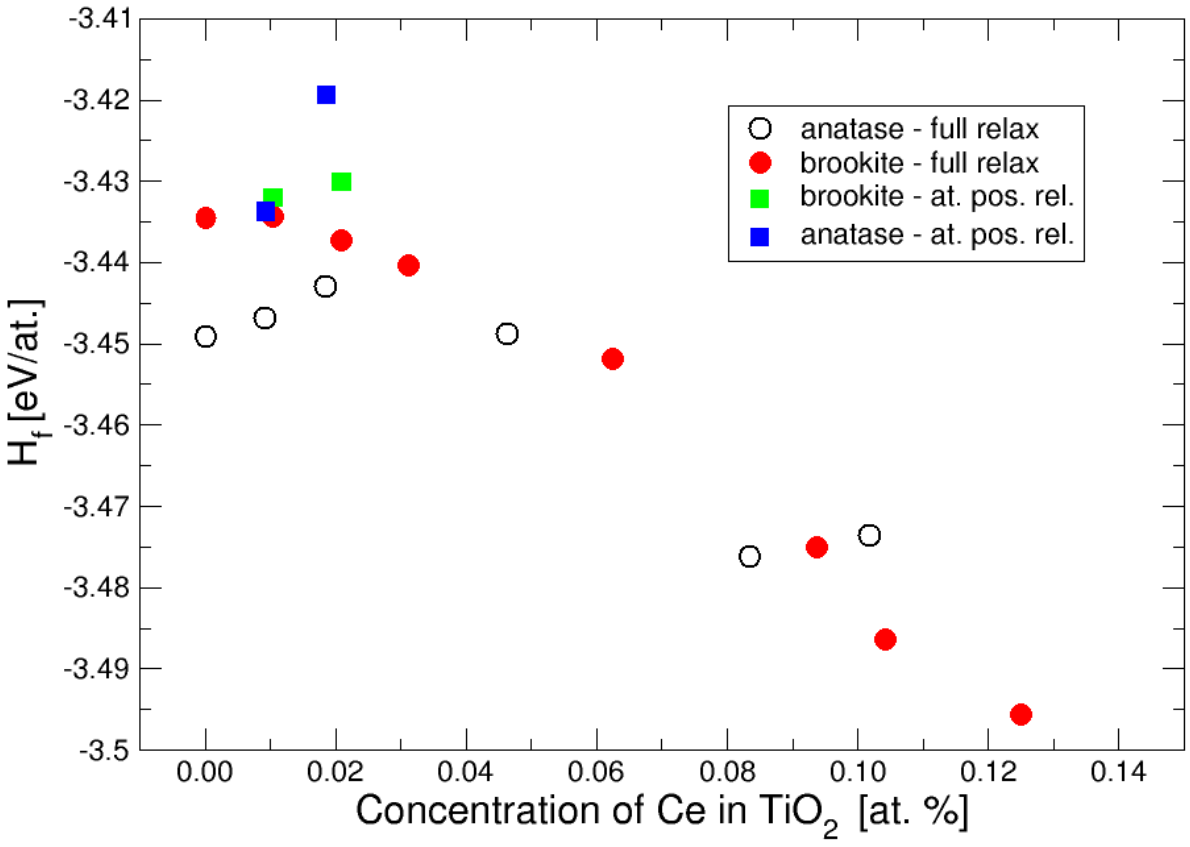

Figure 4: Dependency of enthalpy of formation H_f on concentration of Ce. Again only Ce^{4+} is doped.

In Figure 4, enthalpy of formation as a dependence of concentration of cerium is shown for anatase and brookite. Two models were considered. At first we fixed the lattice constants for the pure brookite and anatase phase for selected cerium concentrations, i.e. ca. 1% and 2% at. (blue squares for anatase and green squares for brookite). The solid red circles and empty spheres denote concentrations of brookite and anatase, where all degrees of freedom were relaxed.

Enthalpy of formation of pure anatase is 15 meV/at. lower than H_f of brookite. This corresponds with theoretical estimation 25 meV/at. derived from enthalpy of transformation. [26] Even for low concentration, the scattering of H_f is not a suitable model. Up to 2% at. of Ce, anatase is clearly more stable, whereas between 2% at. and 10% at. the H_f is very similar and therefore the probability of cerium entering both phases is very similar as well. At higher concentration the brookite phase is lower, indicating that it is the dominant phase cerium will enter.

3.3.2 Effect of Pressure

Besides from studying the dependence of enthalpy of formation on concentration, we also investigated the dependence of enthalpy of formation on applied pressure, see Figure 5. As we can see, the dependency of H_f on pressure is linear for both anatase and brookite, pristine or doped, i.e. decreasing with increasing pressure. The difference between H_f for selected concentrations of Ce is constant under this small pressure. It is probably because the applied pressure is rather low. We assume that bigger pressure would show non-linear dependency. At least our results show that the enthalpy of formation is pressure-dependent.

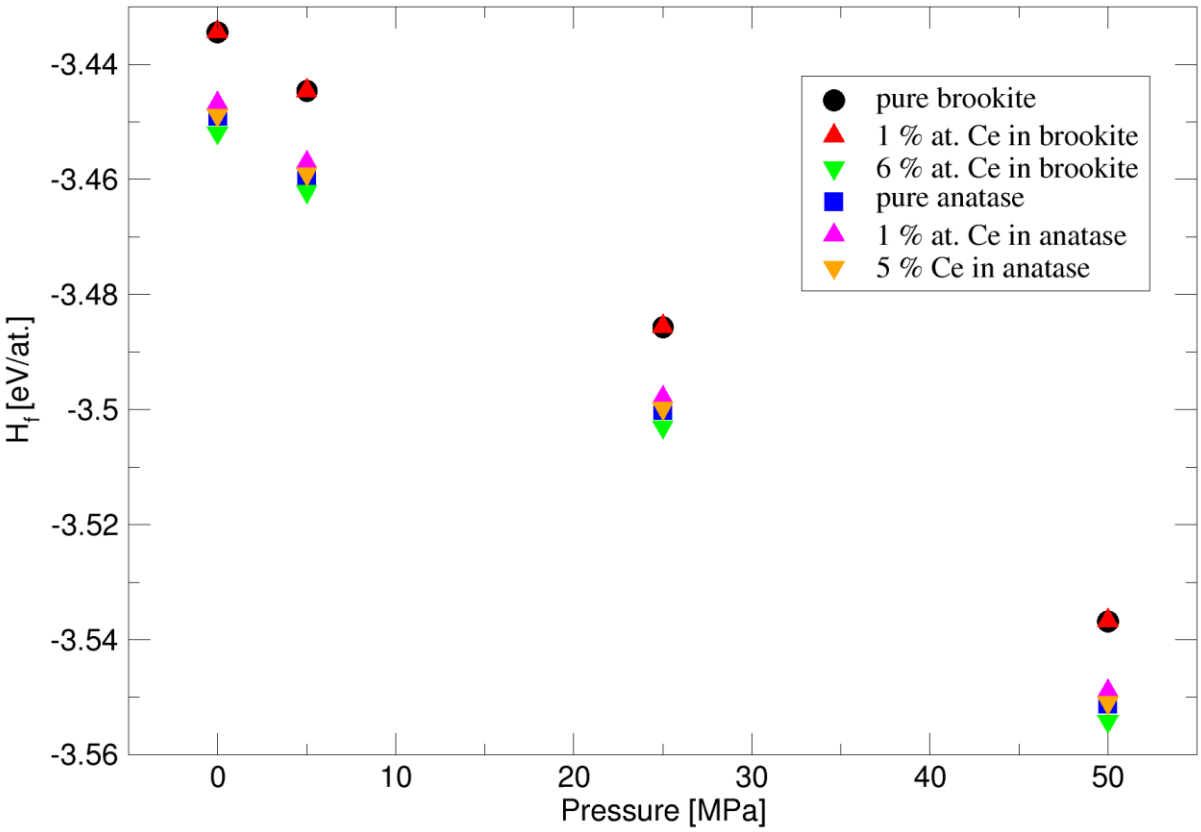

Figure 5: Dependency of enthalpy of formation on applied pressure.

3.4. Cerium Dioxide

Cerium dioxide in a cubic structure, space group Fm-3m (225), [30] is a stable phase that would occur, if all titanium atoms would be replaced by cerium. We investigated the total energy as a function of volume in cerium dioxide.

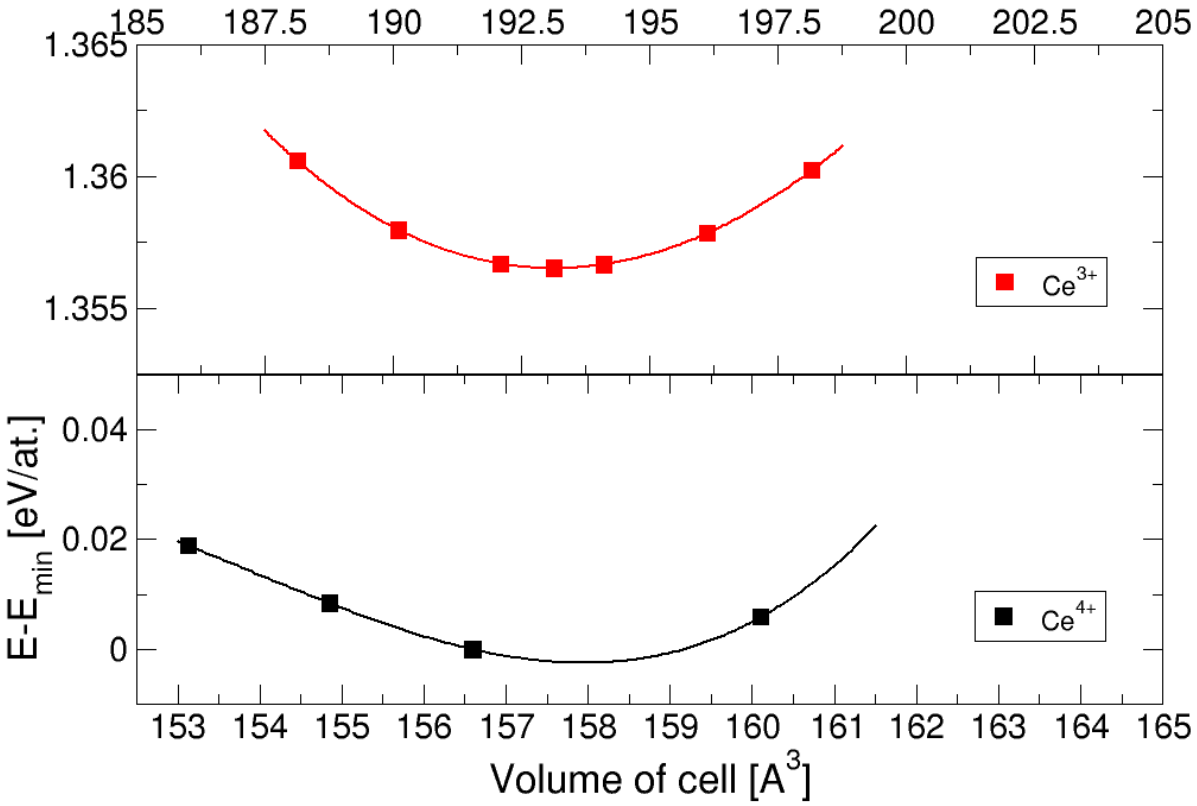

Figure 6: Energy volume curves of CeO_2 with Ce^{3+} only (red) and Ce^{4+} only (black).

3.5. Other Titanates

In the process of synthesis of TiO_2 doped with Ce, there are many possible compounds which can occur, some of them stoichiometric, but even non-stoichiometric ones. One of them seems to be very promising in photocatalysis – $CeTiO_4$ which has been observed quite recently and is not yet well-described. [27]

In order to make sure our results are reliable, we computed phases which are in fact very similar, namely $LaTaO_4$ and $CeTaO_4$. $LaTaO_4$ is a prototype structure, existing in both monoclinic and orthorhombic phases. It may not seem to have much in common with $CeTiO_4$ but it has nearly the same electronic structure, because Ta has one more valence electron more than Ti and La has one electron less than Ce, so they compensate. $CeTaO_4$ has only one more valence electron than $CeTiO_4$.

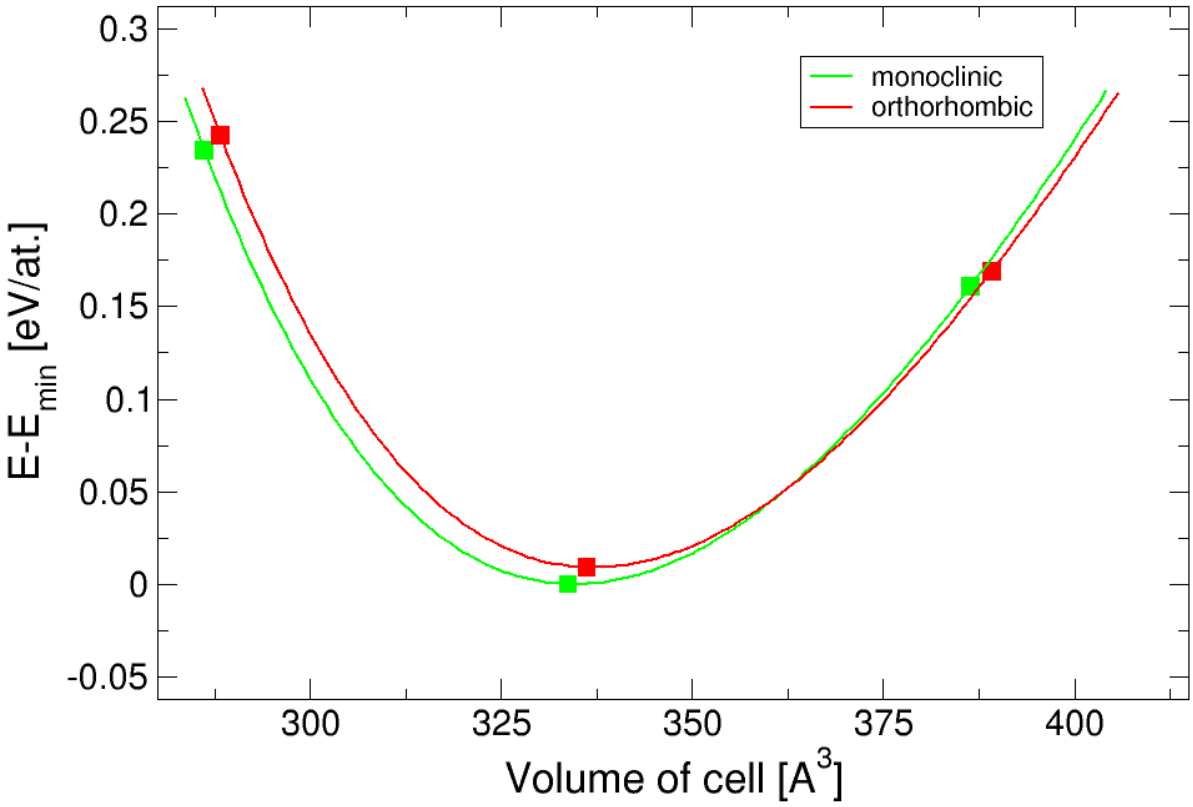

Figure 7: $LaTaO_4$ – energy-volume curves for monoclinic and orthorhombic structures.

The total energy of the monoclinic phase is slightly lower (ca. 10 meV), then the orthorhombic phase. For certain higher volume, the stability of the structure is reversed, the orthorhombic one is preferred over the monoclinic, see Figure 7. The calculated lattice constants for both structures are in good agreement with the experiment, see Table 4 for comparison. [29]

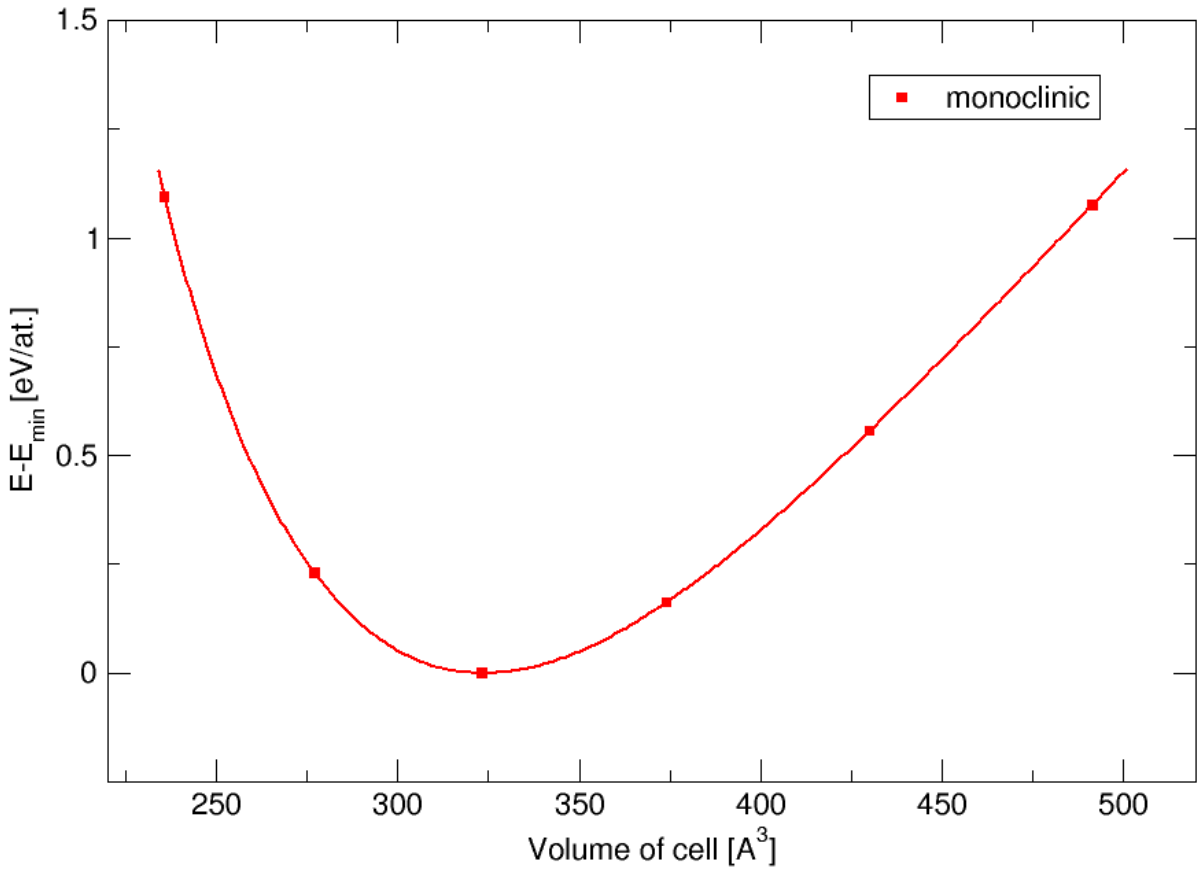

Figure 8: $CeTaO_4$ – energy-volume curve for monoclinic phase.

In the case of $CeTaO_4$, we calculated the monoclinic phase as a function of volume, see Figure 8. We were not able to converge the calculation for the orthorhombic phase, which is in accord that it was never observed experimentally.

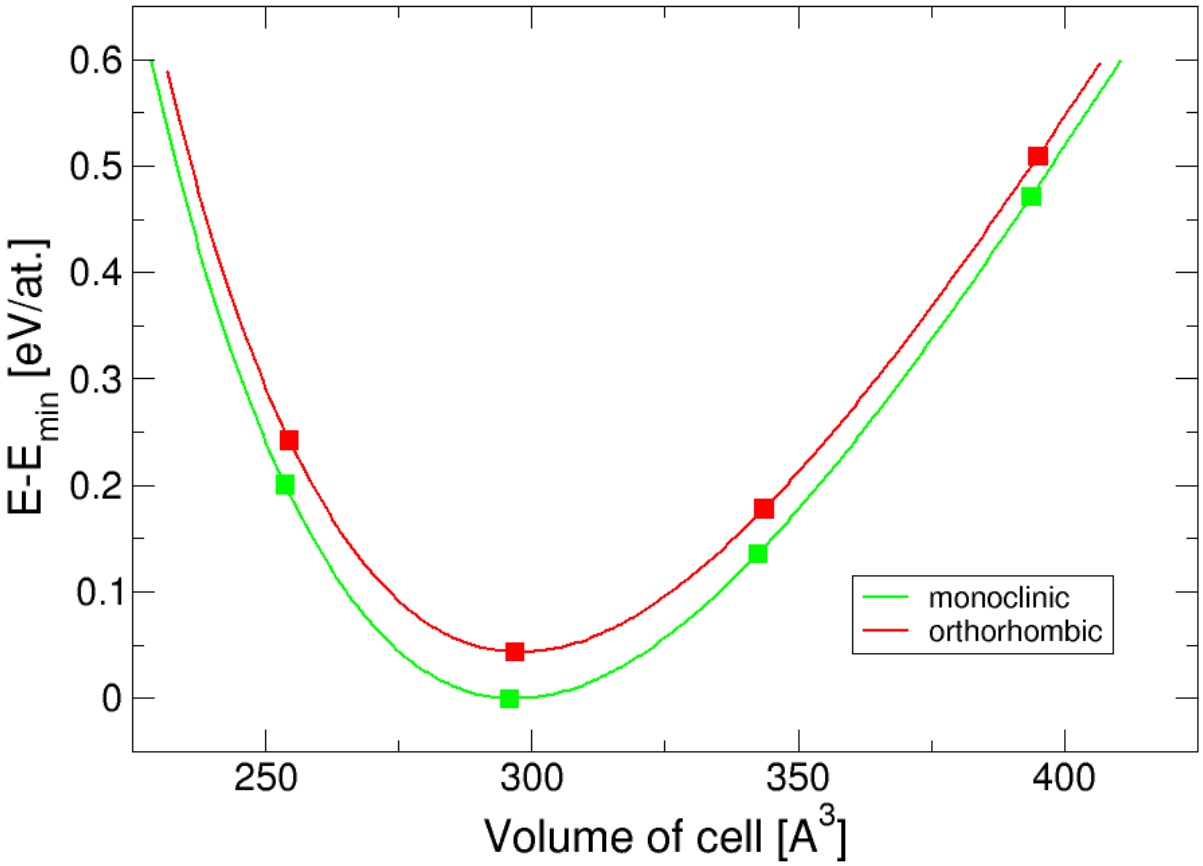

Figure 9: $CeTiO_4$ – energy-volume curves for both monoclinic and orthorhombic phases.

As the prototype structure $LaTaO_4$ exists in both orthorhombic and monoclinic structure, we calculated total energies as a function of volume for both these phases for $CeTiO_4$ as well, see Figure 9. The monoclinic phase is preferred over the orthorhombic one by 40 meV per atom, similarly as in LaTaO4. The energy difference in $CeTiO_4$ between monoclinic and orthorhombic structure is 4x larger than in LaTaO4.

	a [Å]	b [Å]	c [Å]	Angle [°]	Hf [eV/atom]
CeTaO4					
monoclinic	7.72 (7.62)	5.47 (5.53)	7.77 (7.77)	100.07 (100.94)	-3.16
CeTiO4					
monoclinic	7.54	5.29	7.50	99.15	-3.12
orthorhombic	5.35	14.61	3.80	90.00	-3.08
LaTaO4					
monoclinic	7.75 (7.63)	5.59 (5.58)	7.85 (7.82)	101.18 (101.53)	-3.27
orthorhombic	5.66 (5.64)	14.95 (14.72)	3.97 (3.94)	90.00 (90.00)	-3.26

Table 4: Lattice parametres and enthalpy of formation for $CeTaO_4$, $CeTiO_4$ and $LaTaO_4$. The experimental values are in brackets. [28,29]

3.5.1 DOS and Optical Properties of $CeTiO_4$

We analyzed the electronic structure by means of density of states. The DOS of monoclinic and orthorhombic phase of $CeTiO_4$ are depicted in Figures 10, 11. In these figures, the highest occupied levels are marked by zero. Both structures have the highest occupied states composed mainly by titanium and cerium atoms. The monoclinic structure has higher band gap and the dominant part of unoccupied levels come from titanium and cerium, whereas in orthorhombic phase the unoccupied levels are composed mainly by oxygen.

The complex permittivity tensor is the function of energy that was calculated for the monoclinic and orthorhombic structures, see Figures 12 and 13. In both materials strong absorption is in the range 3-10 eV, see the imaginary part (ε_2) in Figures 12, 13.

Energy-loss function and reflectivity were obtained from calculated complex permittivity tensor only for one diagonal element ε_{xx} for both monoclinic and orthorhombic phases.

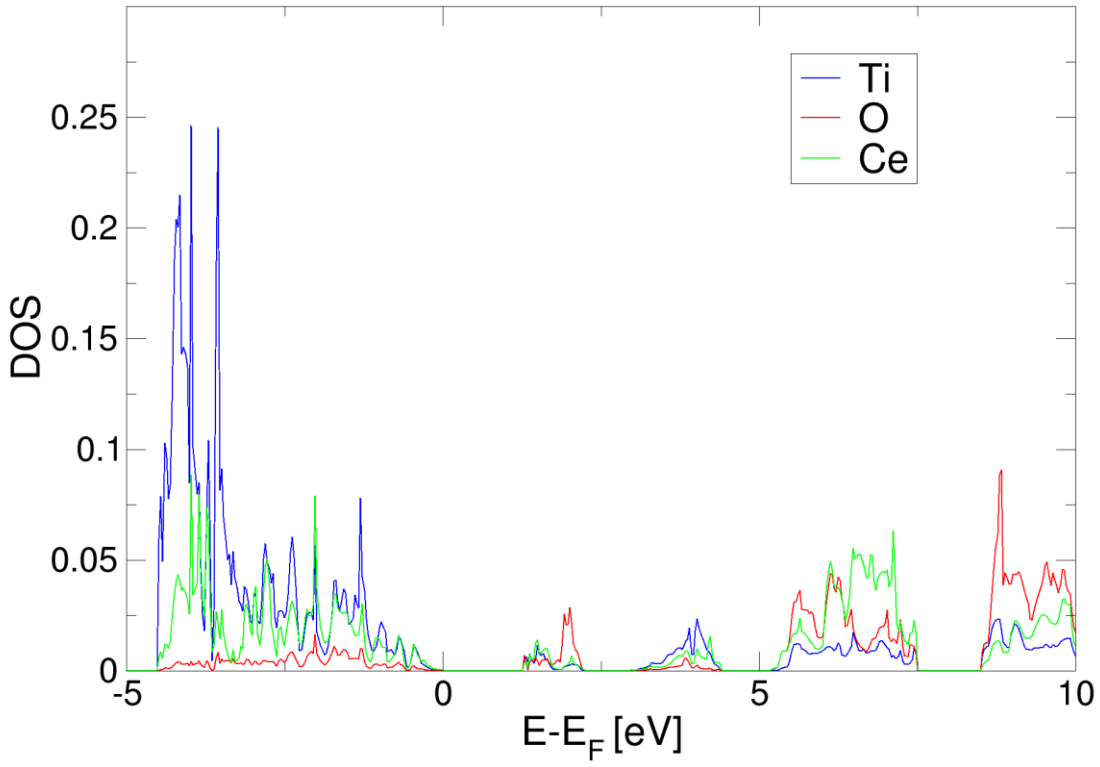

Figure 10: DOS of orthorhombic $CeTiO_4$

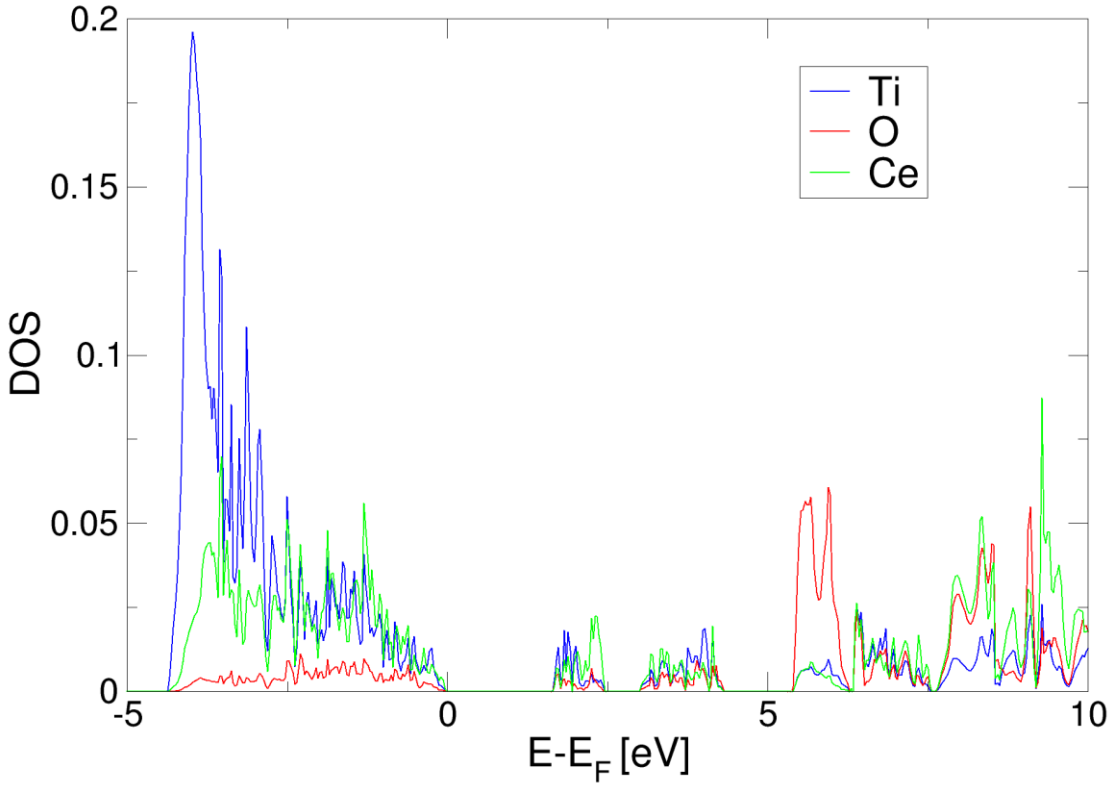

Figure 11: DOS of monoclinic $CeTiO_4$

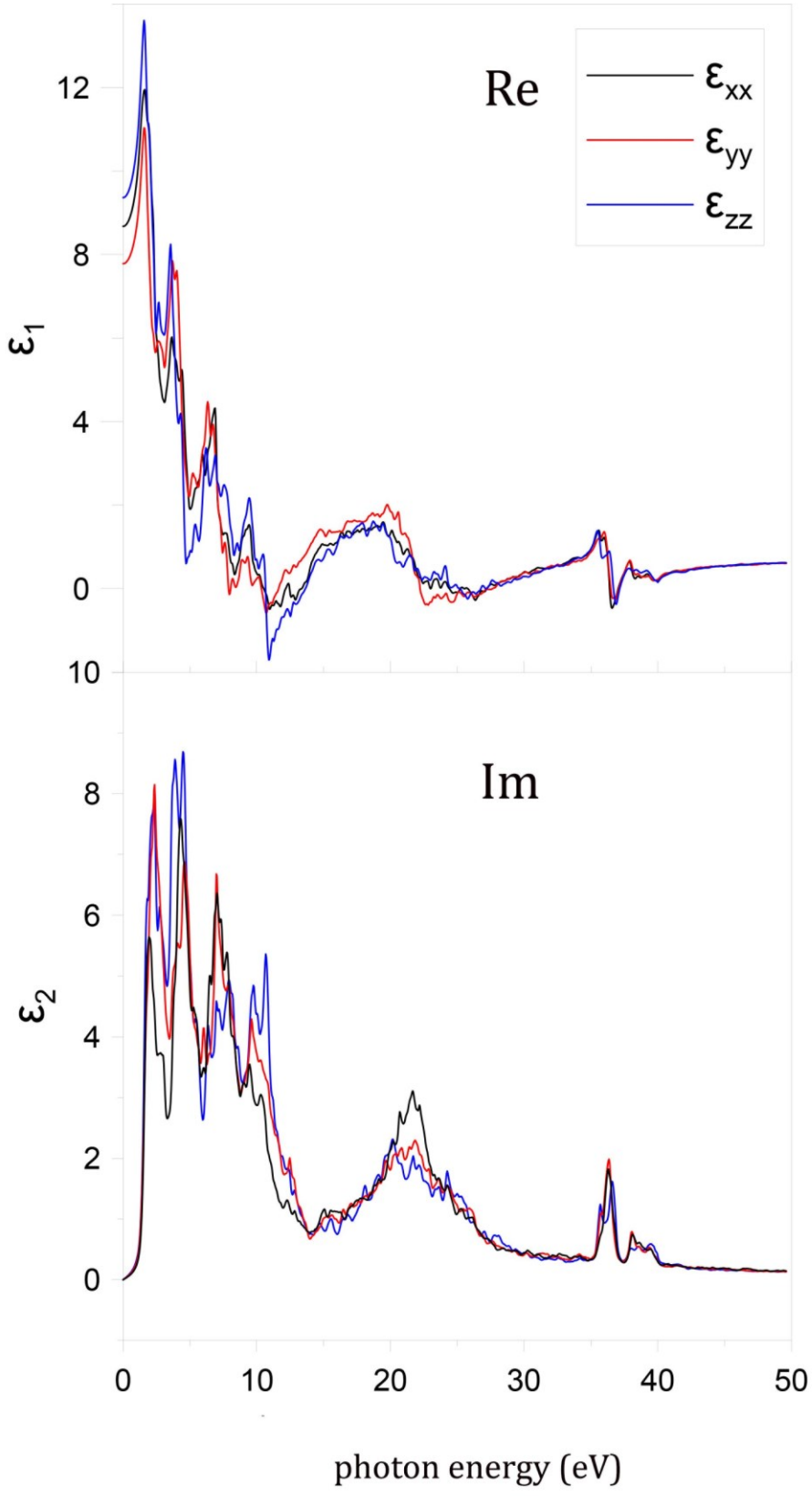

Figure 12: Dielectric tensor (permittivity tensor) of orthorhombic $CeTiO_4$

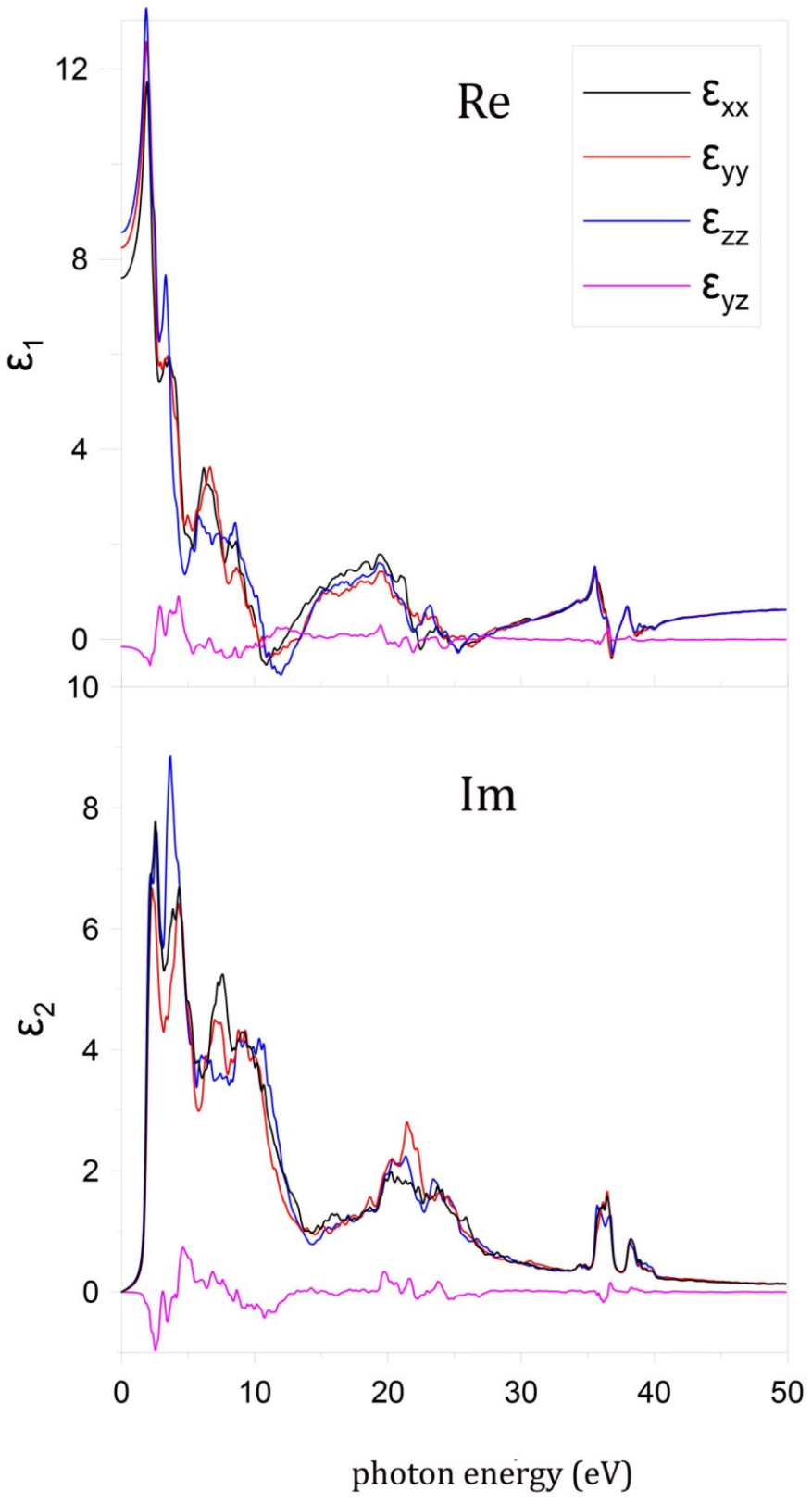

Figure 13: Dielectric tensor (permittivity tensor) of monoclinic $CeTiO_4$

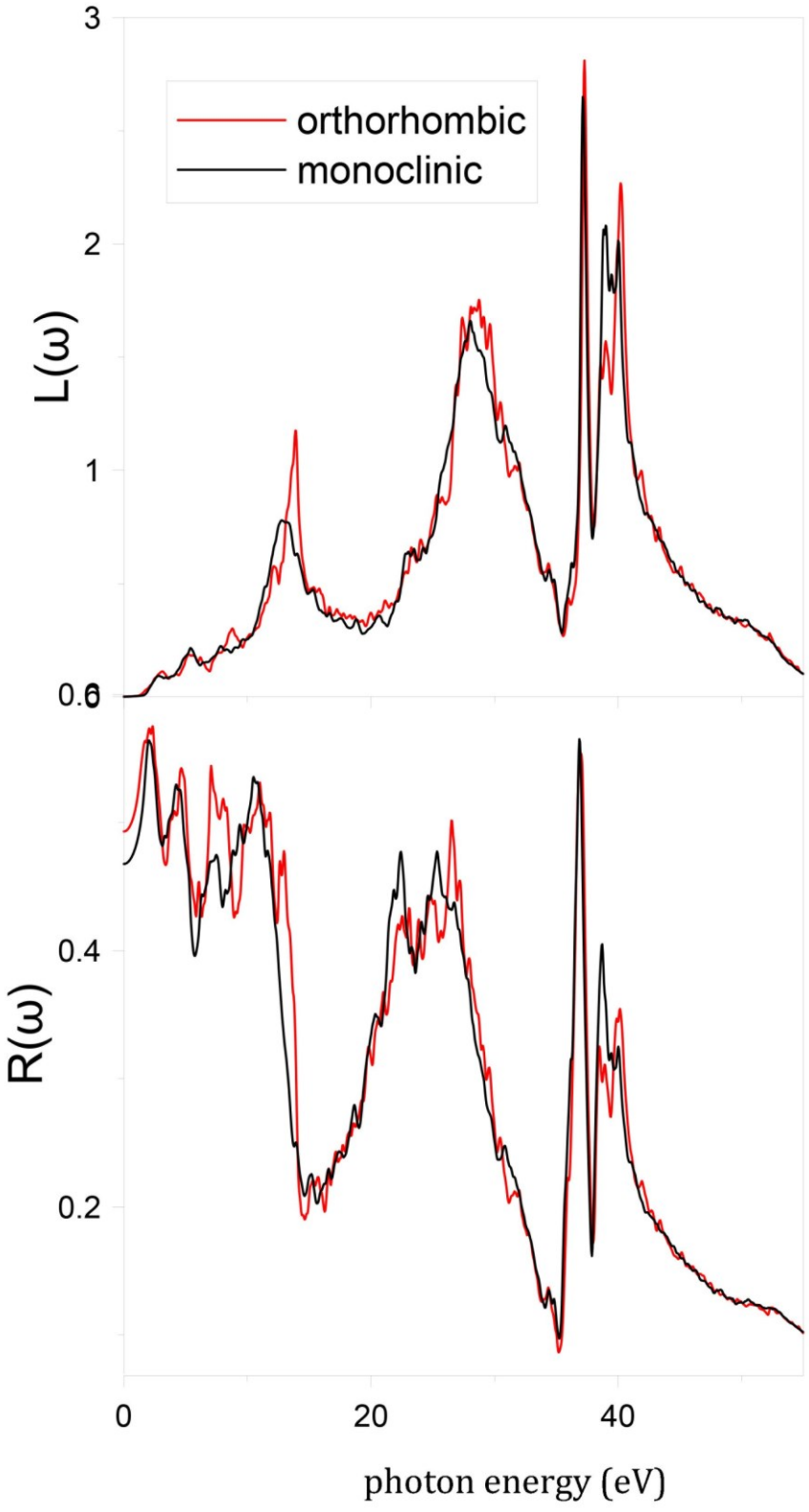

Figure 14: Energy-loss function and reflectivity of monoclinic and orthorhombic phases of $CeTiO_4$

4. Conclusions

We investigated the effect of cerium on the energetic stability of both anatase and brookite phases. The calculated enthalpy of formation indicates the most probable phase for the cerium to enter, as a function of concentration. We studied also the stability of cerium-doped titanates under pressure as motivated by the experimental colleagues.

For the first time we determined the ground-state and lattice parametres of the new found photocatalyst $CeTiO_4$. The monoclinic structure is preferred with respect to orthorhombic one as in the case of prototype structure $LaTaO_4$. The electronic structure and optical properties (frequency-dependent permittivity tensor, reflectivity and energy-loss function) were calculated as well.

In future we would like to investigate the optical properties, mechanical properties and thermal properties of the surface structures of cerium-based titanates.

References

[1] M. Landmann, E. Rauls, W.G. Schmidt, J. Phys.: Condens. Matter **24**, 195503 (2012).

[2] M. Zhi-Gang, W. Yi, S. Shunli, L. Zi-Kui, Comp. Mat. Sci. **83**, 114-119 (2014).

[3] A. Fujishima, X. Zhang, D.A. Tryk, Surf. Sci. Rep. **63**, 515-582 (2008).

[4] T. Ozawa, M. Iwasaki, H. Tada, T. Akita, K. Tanaka, S. Ito, J. Colloid Interface Sci. **281**, 510 (2005).

[5] A.L. Linsebigler, G.Q. Lu, J.T. Yates, Chem. Rev. **95**, 735 (1995).

[6] M.V. Dozzi, E. Selli, J. Photochem. Photobiol. C: Photochemistry Rewievs **14**, 13 (2013).

[7] A. Rapsomanikis, A. Apostolopoulou, E. Stathatos, P. Lianos, J. Photochem. Photobiol. A: Chemistry **280**, 46-53 (2014).

[8] A. Paulenova, S.E. Creager, J.D. Navratil, Y. Wei, J. Power Sources **109**, 431-438 (2002).

[9] D.D. Vvedensky, Quantum theory of electrons in solids (London: Imperial College), (2000).

[10] M. Born, R. Oppenheimer, Ann. Physik **84**, 457 (1927).

[11] M. Born, K. Huang, Dynamical Theory of Crystal Lattices (Oxford: Clarendon Press), pp. 166-169 (1954).

[12] P. Hohenberg, W. Kohn, Phys. Rev. **136**, B864 (1964).

[13] W. Kohn, L.J. Sham, Phys. Rev. **140**, A1133 (1965).

[14] J.P. Perdew, K. Burke, M. Ernzerhof, Phys. Rev. Lett. **77** (1996).

[15] J.C. Slater, Phys. Rev. **51**, 846 (1937).

[16] V. Heine, Solid State Physics (New York: Academic), pp. 1-36 (1970).

[17] G. Kresse, M. Marsman, J. Furthmuller, VASP the Guide (Vienna, Wien Uni), (2014). http://cms.mpi.univie.ac.at/VASP/

[18] G. Grimvall, Thermophysical Properties of Materials (Stockholm: Elsevier), (1999).

[19] O. Stenzel, The Physics of Thin Film Optical Spectra (Berlin: Springer) (2005).

[20] D. Legut, U.D. Wdowik, P. Kurtyka, Mater. Chem. Phys. **147**, 42-49 (2014).

[21] H.J. Monkhorst, J.D. Pack, Phys. Rev. B **13**, 5188 (1976).

[22] D.C. Koskimaki, K.A. Gschneidner, N.T. Panousis, J. Cryst. Growth **22**, 225-229 (1974).

[23] Ch. Kittel, Introduction to Solid State Physics (New York: J. Wiley) (1996).

[24] M. Horn, C.F. Schwerdtfeger, E.P. Meagher, Zeitschrift fuer Krystalographie **136**, 273 (1977).

[25] D. Dambournet *et. al.*, Inorganic Chemistry **50**, 5855 (2011).

[26] T. Mitsuhashi, O.J. Kleppa, J. Am. Ceram. Soc. **62**, 356 (1979).

[27] S. Otsuka, Yao, Matsuo, J, All. Com. **376**, 262-267 (2004)

[28] A. Santoro, M. Marezio, R.S. Roth, D. Minor, J. Sol. St. Chem. 167-175 (1980).

[29] F. Vullum, F. Nitsche, S.M. Selbach, T. Grande, J. Sol. St. Chem. **181**, 2580-2585 (2008).

[30] N.V. Skorodumova, *et.al.*, Phys. Rev. B **64**, 115108 (2001).

Acknowledgements

I am heartily thankful to my supervisor, Ing. Dominik Legut, Ph.D. from IT4Innovations Centre, VSB – TU Ostrava, whose support and guidance enabled me to develop an understanding of an interesting part of materials science. I also want to appreciate valuable advice from Bc. Barbora Kacerovská.

The fruitful discussion with Ing. Lenka Matějová, Ph.D. is gratefully acknowledged. The financial support of the Grant Agency of the Czech Republic (project reg. No. 14-23274S) is also very much appreciated.

This work was supported by the IT4Innovations Centre of Excellence project (CZ.1.05/1.1.00/02.0070), funded by the European Regional Development Fund and the national budget of the Czech Republic via the Research and Development for Innovations Operational Programme, as well as Czech Ministry of Education, Youth and Sports via the project Large Research, Development and Innovations Infrastructures (LM2011033).